Entropic trapping and electrophoretic drift of a polyelectrolyte down a channel with a periodically oscillating width

Grant I. Nixon and Gary W. Slater*
Department of Physics, University of Ottawa, 150 Louis Pasteur, Ottawa, Ontario, Canada K1N 6N5
(Received 10 July 1995)

We consider the electrophoretic drift of a polyelectrolyte (such as DNA) in a narrow channel or capillary with a spatially varying bore size (this can be thought of as a simplified gel model). These bore-size variations reduce the migration pathway to a series of pores and strictures creating an entropic potential surface through which the polyelectrolyte must migrate. The frequency of barrier crossing (probability of jumping to an adjacent pore) is described as an activated process that is dependent on the change in confinement entropy and on the electrostatic potential energy. At low field intensities, the strictures induce an entropic-trapping regime where the time between traps is a strong function of the molecular size; our simulations corroborate our analytic results. Moreover, we examine two critical field intensities: the first, ε_μ, is the field intensity beyond which the entropic barriers are overcome in an inhomogeneous system, while the other, ε_D, is that for which the longitudinal diffusion coefficient is a maximum.

PACS number(s): 82.45.+z, 83.10.Nn, 87.15.−v, 66.10.Cb

I. INTRODUCTION

The dynamical properties of macromolecules in porous media are immediately relevant to many situations of practical importance including filtration, oil recovery, size exclusion chromatography, transport of solute through membranes, and the Human Genome Project where electrophoretic processes are used to separate DNA fragments of various sizes [1].

The nature of the interactions between DNA and the separation media during electrophoresis is yet poorly understood. This has limited our understanding as to which transport mechanisms are best suited for effective separation of nucleic acids. Although sieving is believed to be the main mechanism in the case of smaller macromolecules [2], in many cases, however, a number of transport mechanisms (e.g., Rouse dynamics [3], reptation [4,5], geometration [6], and self-similar hernias [7]) may be involved. Recently, many authors [8–13] have investigated the phenomenon of entropic trapping. Entropic barrier transport applies to cases in which the equilibrium dimensions of the macromolecules are comparable to the mean pore size of the medium. Typically, entropic trapping is manifested in the form of a diffusion coefficient [8–11], or an electrophoretic mobility [11–13], which is more strongly molecular size dependent than either the Rouse or reptation predictions. We will investigate the manifestation of entropic traps in our model system of strictures and pores and, of relevance to electrophoresis, we will also introduce two critical field intensities ε_μ and ε_D; ε_μ is the field intensity for which the electric forces can overcome the entropic barriers and ε_D is the field intensity for which the longitudinal diffusion coefficient reaches a maximum.

This paper is organized as follows. First, we describe our model system in Sec. II A and our Brownian dynamics algorithm throughout Secs. II B–II E. We then follow with a simplified analytical investigation of our entropic-trapping model in Sec. III. Simulation results follow in Sec. IV, and we conclude in Sec. V by examining the experimental significance of our results.

II. SIMULATION METHODOLOGY

A. The system under study

Our two-dimensional (2D) system is comprised of an infinite channel with semicircular protrusions extending inwardly from the opposing walls (see Figs. 1 and 2). We assume the protrusions to be easily permeated by the solvent ions but completely impermeable to the polyelectrolytes;

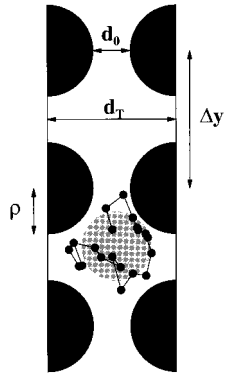

FIG. 1. Computer simulation snapshot of a $M=20$ bead chain in a channel with maximum diameter $d_T=2.8$, minimum diameter $d_0=0.8$, protrusion radius $\rho=1$, and interpore spacing $|\Delta y|=3$. The gray-shaded region is a circle whose radius is equal to the chain's radius of gyration ($r_g\approx 0.76$) and is centered about the chain's center of mass $r_{\text{c.m.}}$. As the chain is essentially unperturbed within the porelike regions (i.e. $2r_{g0}<d_T$), the chain must first be compressed before passage through a stricture becomes possible.

* Author to whom correspondence should be addressed. Electronic address: gary@physics.uottawa.ca

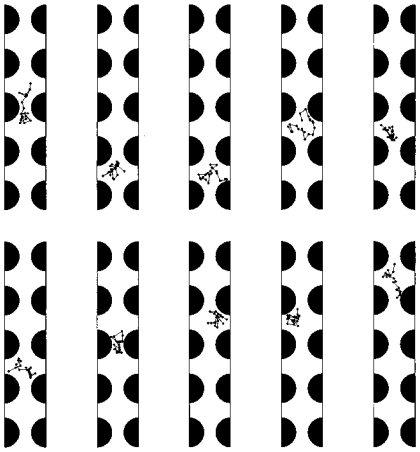

FIG. 2. From upper left to bottom right: computer simulation snapshots of a $M=20$ bead chain migrating in a rough tube (with maximum diameter $d_T=2.8$, minimum diameter $d_0=0.8$, protrusion radius $\rho=1$, and interpore spacing $|\Delta y|=3$) under the effect of a weak field $\varepsilon=0.005$ directed upward. Figure 1 is represented in the fourth frame. The unperturbed radius of gyration for the $M=20$ bead chain is $r_{g0}\approx 0.73$; thus the chain is essentially unperturbed within the porelike regions (i.e., $2r_{g0}<d_T$) while, in the stricture regions, we have compression since $2r_{g0}>d_0$. The (dimensionless) time between frames is $\Delta\tau=310$.

thus the electric field intensity is to be assumed constant throughout. The strictures have both a well-defined periodicity and size, which facilitates the theoretical analysis. The more general case of a random distribution of strictures is currently under study. Note, however, that our strictures are not made up of narrow, flat channels, as was the case in previous studies [10]; we will see later that these channels, besides being somewhat more realistic, lead to qualitatively different physics in the presence of an electric field. We now adopt the following notation to describe our system. The (maximum) tube diameter is d_T, while the radius and periodicity of the semicircular protrusions are ρ and $|\Delta y|$, respectively, with $2\rho<\{|\Delta y|,d_T\}$. Therefore, the minimum channel width is $d_0=d_T-2\rho$. For the purpose of this study, we will be interested in the dynamics of polymers with an unperturbed radius of gyration r_{g0} in the range $d_0<2r_{g0}<\{|\Delta y|,d_T,2\rho\}$ such that the conformations of the polyelectrolytes are relatively unperturbed inside the open (porous) regions whereas they are squeezed (but entirely contained) inside the narrow channels.

B. Brownian dynamics

We employ a modified 2D version of the Rouse model that describes a free-draining polymer chain as a succession of M "beads" at positions $\mathbf{R}_1,\mathbf{R}_2,\ldots,\mathbf{R}_M$ separated by $M-1$ "entropic springs"; each spring represents a sequence of N Kuhn statistical segments of length a. As is customary, we neglect excluded volume and hydrodynamic effects and we work in the *strong-damping limit* of Brownian dynamics (inertial terms are ignored). We may thus write our equation of motion for bead n $(n=1,2,\ldots,M)$ in the generalized (position) Langevin form

$$\zeta\frac{d\mathbf{R}_n}{dt}=(1-\delta_{n,M})\mathbf{F}_s(n+1,n)+(1-\delta_{n,1})\mathbf{F}_s(n-1,n)+\sum_{\text{constr}}\mathbf{F}_{\text{constr}}+q\mathbf{E}+\mathbf{f}_n(t), \tag{1}$$

where ζ is the friction coefficient of a single bead, $\mathbf{R}_n$ is the bead position, $\mathbf{F}_s(m,n)$ is the entropic spring force on bead n due to bead m, $\delta_{i,j}$ is a Kronecker delta function, $\mathbf{F}_{\text{constr}}$ is the force on bead n due to an external constraint (e.g., the tube wall), $q\mathbf{E}$ is the force due to the electric field $\mathbf{E}$ acting on the charge q of the bead, and $\mathbf{f}_n$ is the stochastic force acting on bead n. The stochastic (Langevin) force $\mathbf{f}_n$ is characterized by the moments

$$\langle f_{n\alpha}(t)\rangle=0,$$
$$\langle f_{n\alpha}(t)f_{m\beta}(t')\rangle=2\zeta k_BT\delta_{nm}\delta_{\alpha\beta}\delta(t-t'), \tag{2}$$

with $\{\alpha,\beta\}=\{x,y\}$ being a coordinate designation (x and y are orthogonal). One must discretize these equations and render them into dimensionless form. From Eq. (2), we can establish the relation

$$\langle f_{n\alpha}^2(t)\rangle=\frac{2\zeta k_BT}{\Delta t}, \tag{3}$$

where Δt is the correlation time of the stochastic force (i.e., our integration time step). The stochastic force $f_{n\alpha}$ is chosen such as to obey the Gaussian distribution

$$P(f_{n\alpha})df_{n\alpha}=\frac{1}{\sqrt{2\pi\langle f_{n\alpha}^2\rangle}}\exp\left(-\frac{f_{n\alpha}^2}{2\langle f_{n\alpha}^2\rangle}\right)df_{n\alpha}. \tag{4}$$

Let us implicitly define the dimensionless stochastic vector $\eta_n=(\eta_{nx},\eta_{ny})$, viz.,

$$f_{n\alpha}(t)=\left(\frac{2\zeta k_BT}{\Delta t}\right)^{1/2}\eta_{n\alpha}(t), \tag{5}$$

where $\eta_{n\alpha}$ is Gaussian distributed with zero mean and unit variance

$$\langle\eta_{n\alpha}(t)\rangle=0,\quad\langle\eta_{n\alpha}^2(t)\rangle=1. \tag{6}$$

If we now define the natural units

$$f_L=\frac{2k_BT}{L},\quad\tau_L=\frac{\zeta L^2}{2k_BT},\quad L=Na \tag{7}$$

for force, time, and length ($L=Na$ being the maximum possible spring extension), respectively, the equation of motion can be rewritten in the scaled and discretized two-dimensional form

$$\Delta\mathbf{r}_n(\tau)=\Delta\tau\left[(1-\delta_{n,M})\mathbf{f}_s(n+1,n)+(1-\delta_{n,1})\mathbf{f}_s(n-1,n)+\sum_{\text{constr}}\mathbf{f}_{\text{constr}}+\boldsymbol{\varepsilon}\right]+\sqrt{\Delta\tau}\,[\eta_{nx}(\tau)\mathbf{e}_x+\eta_{ny}(\tau)\mathbf{e}_y], \tag{8}$$

where $\mathbf{e}_x$ and $\mathbf{e}_y$ are unit vectors along their respective coordinate axes x and y. In Eq. (8), we have also implicitly defined several scaled variables, namely,

$$\frac{\mathbf{R}_n(t)}{L}\rightarrow\mathbf{r}_n(\tau),\quad \frac{\mathbf{F}_s}{f_L}\rightarrow\mathbf{f}_s,\quad \frac{\mathbf{F}_{\text{obst}}}{f_L}\rightarrow\mathbf{f}_{\text{obst}},\quad \frac{q\mathbf{E}}{f_L}\rightarrow\boldsymbol{\varepsilon},$$

$$\frac{t}{\tau_L}\rightarrow\tau,\quad \frac{\Delta t}{\tau_L}\rightarrow\Delta\tau. \tag{9}$$

In the simulation, we compute the forces on all beads and follow with simultaneous displacements $\Delta\mathbf{r}_n$ for all beads ($n=1$ to M). Integration problems can occur when spring extensions tend to values greater than the maximum spring length $L=Na$ or when beads attempt to enter the walls. This requires careful adjustment of the time step $\Delta\tau$ (see Sec. II E). In the rest of this paper, all variables are scaled (dimensionless) variables unless specified otherwise.

C. Entropic springs

The effective contractile force $-F_s$, also known as the entropic spring force, arises from the loss of entropy in the system of N Kuhn statistical segments of length a that comprise a spring (or subchain) when the latter is given an extension Δr. For a d-dimensional subchain where the ends are separated by a *mean distance* Δr, and in the so-called stress ensemble, we have [14]

$$\Delta r=\frac{I_{d/2}(f_a)}{I_{d/2-1}(f_a)}, \tag{10}$$

where I_ν is the modified Bessel function of order ν and $f_a=F_s a/(k_BT)=2f_s/N$. For $d=3$, Eq. (10) reduces to the well-known Langevin function $L(f_a)=\coth(f_a)-1/f_a$. Inverting the Taylor series expansion of Eq. (10) yields the force-extension relation

$$f_s=\frac{Nd}{2}\Delta r\left[1+\frac{d}{(2+d)}(\Delta r)^2+\frac{d^2(8+d)}{(2+d)^2(4+d)}(\Delta r)^4+\cdots\right], \tag{11}$$

from which one yields the general form of the harmonic spring constant

$$k_h=\frac{Nd}{2}\frac{f_L}{L}=d\frac{k_BT}{Na^2}, \tag{12}$$

where we have reintroduced the appropriate dimensional units. While the use of harmonic springs may lead to unphysical stretching [15], the use Eq. (11) is limited due to slow convergence. Consequently, we approximate the expansion using the ''modified Padé approximant'' [14]

$$f_a=\frac{2f_s}{N}\approx\frac{\Delta r[d-(\Delta r)^2]}{1-(\Delta r)^2}, \tag{13}$$

which proves remarkably accurate (the error is less than 6.5% over the whole range of spring extensions for $d=2$) while maintaining the correct asymptotic behaviour for *both* $\Delta r\rightarrow 0$ and $\Delta r\rightarrow 1$.

D. Tube pathway

The tube pathway is divided into two components (constraints): a flat tube and a series of periodic semicircular protrusions extending inwardly from the tube walls. Both are represented by hard cores with a Lennard-Jones-like soft-core repulsive force extending a distance σ from the hard core. If Δr is the distance between the obstacle surface and the pointlike polymer bead, the force is directed perpendicular to the tube pathway surface, viz.,

$$f_{\text{constr}}(\Delta r)\rightarrow\infty\ (\Delta r\leqslant 0), \tag{14}$$

$$f_{\text{constr}}(\Delta r)=A(\Delta r+\sigma)\left[\frac{1}{\Delta r^2+2\sigma\Delta r}-\frac{1}{3\sigma^2}\right]^2 \quad (0<\Delta r<\sigma), \tag{15}$$

$$f_{\text{constr}}(\Delta r)=0\quad (\Delta r\geqslant\sigma). \tag{16}$$

Thus there is no discontinuity at $\Delta r=\sigma$.

E. Adaptive stepsize control

1. Time cutting

Our stochastic differential equation integrator exerts adaptive control over its own progress, making frequent changes in its step size when system integrity violations occur. Such violations result in the time increment $\Delta\tau$ being divided by some convenient value (4 in our implementation) and the step being reattempted. Thus the time increment is not a static quantity, but is reduced in accordance with the stresses built up in the chain. A small time increment $\Delta\tau$ allows the system to tiptoe through rough terrain, while large time increments permit great strides through smooth potential surfaces. Thus the time increment is continuously optimized, which results in significant gains in terms of efficiency. Such an optimization scheme also permits the incorporation of a maximum spatial step size to better suit the dimensions of the system under study. This has proven to be most useful for a recent study of electrophoretic collisions [16].

However, all things being equal, it is clear that $\Delta\tau$ will tend to be smaller when large stochastic forces are chosen since large forces tend to compromise system integrity more often than do small forces. Therefore, large stochastic forces will, on average, receive smaller time increments (i.e., are given less weight) than will smaller stochastic forces. We refer to this time bias as *"stochastic cooling"* since this biasing is tantamount to lowering the temperature of the system.

2. Damping the evolution of the time increment

Fortunately, there is a simple way of sidestepping stochastic cooling problems. If we relax the requirement that every stochastic term receives the same *a priori* amount of integrated time and simply demand that each receives *approxi-*

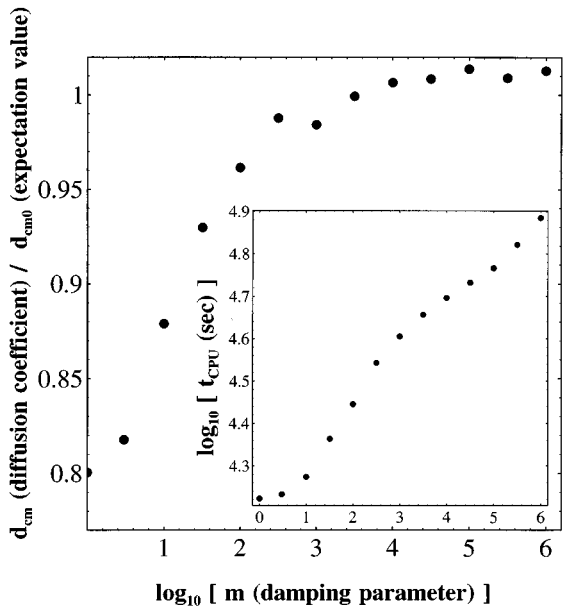

FIG. 3. Effects of the damping parameter m on the diffusion constant $d_{\text{c.m.}}$ for a chain with $M=5$ beads reveal that the critical threshold value of the damping parameter is approximately $m^*=1000$. The effect of m on the process CPU time, as carried out on a SUN model 10 UNIX computer workstation (see inset), reveals that the CPU time is a monotonic, slowly increasing function of the damping parameter m. The settings were no walls, $\Delta\tau_{\max}=0.1$ for the maximum time increment, and $\tau_{\text{sim}}=0.5$ for the total simulation time.

mately the same amount, then stochastic cooling can be averted. There exist a number of ways in which this may be accomplished; we opted to damp the evolution of the time increment. Let us consider a case where a given time step $\Delta\tau_0$ leads to the system correctly performing a time step. The next time increment $\Delta\tau_1$ is then chosen to be

$$\Delta\tau_1=\Delta\tau_0^{(m-1)/m}(\Delta\tau_{\max})^{1/m}, \tag{17}$$

where $\Delta\tau_{\max}$ is a user-defined maximum time increment and the damping parameter m can be chosen large enough to ensure that successive $\Delta\tau_i$'s increase slowly following each time step. Therefore, for simulations with m large, a histogram plot of the net integrated time per bin with respect to the (binned) Langevin forces will, effectively, be equivalent to the probability distribution function of Langevin forces (i.e., the bias will be removed). Moreover, this damping permits residual stresses in the system to relax smoothly while the time increment is being optimized.

3. Effects of the damping parameter

A series of simulations [17] were carried out to determine the relationship between the choice of m and simulation accuracy as well as CPU time. Several different damping factors were chosen for the case of an unperturbed (free) five-bead chain with a maximum time increment $\Delta\tau_{\max}=0.01$. We first examined the effect of m on the accuracy. The results are plotted in Fig. 3. For a $M=5$ bead chain, the self-diffusion coefficient of the center of mass is expected to be $d_{\text{cm}_0}=0.1$ [from Eq. (21)]. As we can see, there is a marked discrepancy between the expected value and the simulation points as m decreases below about $m^*=1000$. Hence, by sufficiently damping the evolution of the time step, we effectively eliminate stochastic cooling. As for the effect of m on CPU process time, the results appear in the inset of Fig. 3. As can be seen, the CPU process time is a monotonic, slowly increasing function of m. Thus one can improve simulation accuracy (i.e., by increasing m) significantly with little penalty with regards to the CPU process time.

III. ANALYTICAL STUDY

A. The free chain

We first review the properties of a free Rouse chain using our scaled units. Consider a freely jointed chain consisting of M beads coupled through $M-1$ springs, with $\langle(\Delta r)^2\rangle_0$ being the mean square spring length. We will use the subscript zero for the unperturbed values of the quantities. The radius of gyration of the polymer r_{g0} is given by [see, e.g., Ref. [18], Eq. (I.5.15)]

$$r_{g_0}^2=\frac{M^2-1}{6M}\langle(\Delta r)^2\rangle_0. \tag{18}$$

The self-diffusion coefficient of the center of mass vector $r_{\text{c.m.}}(t)$ is defined by the relation

$$d_{\text{c.m.}}\equiv\lim_{t\to\infty}\frac{1}{2d}\frac{\langle[r_{\text{c.m.}}(\tau)-r_{\text{c.m.}}(0)]^2\rangle}{\tau}, \tag{19}$$

where d is the dimensionality of the space and the position of the center of mass is given by

$$r_{\text{c.m.}}=\frac{1}{M}\sum_{n=1}^{M}r_n. \tag{20}$$

In the Rouse model, the unperturbed value of the diffusion coefficient is given by

$$d_{\text{c.m.}_0}=\frac{1}{2M}, \tag{21}$$

whereas the Rouse (terminal) relaxation time of the end-to-end vector is

$$\tau_{R_0}=\frac{1}{N}\left(\frac{M}{\pi}\right)^2. \tag{22}$$

As for the mean (free-drift) electrophoretic velocity of the center of mass, it is given by

$$v_{\text{c.m.}_0}=\varepsilon \tag{23}$$

where ε is the scaled field intensity. Thus the (free-drift) electrophoretic mobility $\mu\equiv v_{\text{c.m.}}/\varepsilon$ is given by

$$\mu_0=1. \tag{24}$$

It is indeed because the free-solution electrophoretic mobility is independent of molecular size that electrophoretic separation must be carried out in (e.g., gel-like) ''sieving'' structures.

B. Free electrophoretic drift of a chain

Let us now consider the case of a polyelectrolyte drifting freely in a tube without strictures under the influence of an electric field ε. The unconditional mean first passage time for covering any distance $|\Delta y|$ is simply given by [19]

$$\tau(\delta)=\frac{\tanh[\delta]}{\delta}\tau_0, \tag{25}$$

where the bias factor δ is given by

$$\delta=\frac{v_{\text{c.m.}_0}\tau_0}{|\Delta y|}=M\varepsilon|\Delta y|. \tag{26}$$

Here $v_{\text{c.m.}0}=\varepsilon$ is the velocity given in Eq. (23) while τ_0 is the Brownian time for diffusing over a mean square distance $|\Delta y|^2$,

$$\tau_0=\frac{|\Delta y|^2}{2d_{\text{c.m.}_0}}=M|\Delta y|^2. \tag{27}$$

The corresponding mean first passage times for migrating a distance $|\Delta y|$ in the direction of the field $(+)$ or in the direction opposite to the field $(-)$ are given by the expression

$$\tau_{0\pm}(\delta)=\frac{\pm(1-e^{\mp 2\delta})}{\delta}\tau_0. \tag{28}$$

Note that in the zero-field limit $\delta\to 0$, we have $\tau_{0\pm}\to 2\tau_0$ whereas, in the infinite-field limit $\delta\to\infty$, we yield the limiting values $\tau_{0+}\to\tau_0/\delta=|\Delta y|/v_{\text{c.m.}0}=|\Delta y|/\varepsilon$ and $\tau_{0-}\sim e^{2\delta}\to\infty$, as expected. Thus, in our analysis of our 2D channel with periodic protrusions, lower bounds for both the mean first passage time and the trapping time will be provided by Eqs. (28) and (25), respectively.

C. Trapping of a polymer chain in the absence of fields

The rate of successfully attempted jumps from pore i to pore $i\pm 1$ is expected to depend on the ratio of the (dimensional) activation energy $\Delta G=T\Delta S$, due to the change in confinement entropy ΔS imposed on the chain by the stricture, to the thermal energy k_BT, viz.,

$$\Gamma=\omega(M)e^{-\Delta S/k_B}, \tag{29}$$

where $\omega(M)$ is the size-dependent rate of attempted transitions. The entropy of a polymer molecule being an extensive variable, we have $\Delta S\sim M$. For an ideal random-walk chain and a narrow channel with parallel surfaces, the entropy of confinement scales like $\Delta S\sim(r_{g0}/d_0)^2$, where r_{g0} is the unperturbed radius of gyration and d_0 is the diameter of the channel [20]. Muthukumar and Baumgärtner [10] investigated a grid of (square) porelike regions joined through rectangular bottlenecks (i.e., channels or gates) to clarify the role of entropically activated diffusion in the absence of electric fields. We suggest using semicircular protrusions as a ''more realistic'' model of the narrow channels in, for example, polymer gels. Since the polymer molecule will reach a minimum entropy when its center of mass is located in the middle of the stricture, we can generalize the before-mentioned scaling law using

$$\frac{\Delta S}{k_B}\cong 2\int_0^{r_{g_0}}dy\,P(y)\left(\frac{r_{g_0}}{d(y)}\right)^2, \tag{30}$$

where $d(y)=d_0+2\rho-2(\rho^2-y^2)^{1/2}$ is the channel width at a distance y from the pore center [with $d(0)=d_0$ and $d(y\geqslant\rho)=d_T$] and $P(y)$ is the local monomer density. We implicity assume that $d_T\gg d_0$ and $r_{g0}<\rho$. The full solution of this confinement problem requires a self-consistent calculation of $P(y)$ for the given geometry. However, we can get the correct form of the first two terms by simply assuming that $P(y)$ remains a smooth distribution of width r_{g_0} centered at $y=0$; we obtain

$$\frac{\Delta S}{k_B}\cong\left(\frac{r_{g_0}}{d_0}\right)^2\left[1-b\frac{r_{g_0}^2}{\rho d_0}+\cdots\right], \tag{31}$$

where b is a numerical factor of order unity. The omitted terms also depend on the ratio $d_0/2\rho$, which measures the ''flatness'' of the strictures. We note that the first term (prefactor) is the expected result for a flat channel, as discussed previously. The second term (first correction term) is proportional to $r_{g0}/(\rho d_0)^{1/2}$, the expansion parameter of the series; this is the relative span of the polymer molecule when it is centered about the point of minimum width d_0 in the channel. Obviously, we would recover the results of Muthukumar and Baumgärtner in the limit of flat channels (i.e., when $\rho\to\infty$) as the second term would then vanish. When d_0 is small, those monomers not situated in the stricture's narrowest section are less confined and the average channel width experienced is somewhat larger than d_0; hence the loss of conformational entropy is reduced. Interestingly enough, the critical radius of gyration above which this effect is significant is given by the geometric mean $(\rho d_0)^{1/2}$ of the two characteristic lengths describing the strictures. Since the unperturbed radius of gyration scales as $r_{g_0}\sim M^{1/2}$, we may combine Eqs. (29) and (31) to yield

$$\Gamma\approx\omega(M)\exp\left[-\frac{\phi M}{d_0^2}\left(1-\frac{\theta M}{\rho d_0}\right)\right], \tag{32}$$

where ϕ and θ are topological constants that take into account, among other things, the average length of the springs of the model polymer. The frequency $\omega(M)$ is given by $1/\tau_0$, where the mean diffusion time τ_0 is given by Eq. (27). Thus we have

$$\frac{d_{\text{c.m.}0}}{d_{\text{c.m.}}}=\frac{\tau_{\text{trap}}}{\tau_0}=\frac{1}{\Gamma\tau_0}\approx\exp\left[\frac{\phi M}{d_0^2}\left(1-\frac{\theta M}{\rho d_0}\right)\right] \tag{33}$$

for the mean trapping time (i.e., the mean time between pore-to-pore transitions) and the (scaled) diffusion coefficient $d_{\text{c.m.}}=(\Delta y)^2/(2\tau_{\text{trap}})$, where $d_{\text{c.m.}0}$ is given by Eq. (21).

D. Application to electrophoresis

For low field intensities E (dimensional), the rate of successfully attempted jumps from pore i to pore $i\pm1$ will also depend on the work performed, viz.,

$$\Gamma_{i\to i\pm1}\approx\exp\left[-\frac{T\Delta S+\Delta W}{k_BT}\right], \tag{34}$$

where $\Delta W=\mp QE|\Delta Y|L/2$ and $Q=Mq$ is the net charge of the polyelectrolyte. Therefore, the electric field effectively lowers the energy barrier in the field direction while simultaneously increasing the energy barrier in the direction opposite the field. Using the results of Sec. III C, we may now write the trapping time as

$$\frac{\tau_{\text{trap}\pm}}{2\tau_0}\approx\exp\{M|\Delta y|[\epsilon_\mu(M)\mp\varepsilon]\}, \tag{35}$$

where we distinguish between the forward $(+)$ and backward $(-)$ trapping times $\tau_{\text{trap}\pm}$ when the field ε is directed in the $+y$ direction. We have also implicitly defined the critical (mobility) field

$$\epsilon_\mu(M)\approx\frac{\phi}{|\Delta y|d_0^2}\left[1-\frac{\theta M}{\rho d_0}\right] \tag{36}$$

above which the electric forces overcome the entropic forces. We note that $\epsilon_\mu(M)$ decreases with molecular size M if the narrow channels are not flat (i.e., if ρ is not infinite). In other words, flat channels are *qualitatively* different because the critical field necessary to overcome entropic barriers would then be given by the prefactor in Eq. (36) and, consequently, be independent of molecular size. When $\varepsilon\gg\epsilon_\mu(M)$, the effect of the strictures should become negligible and one should recover the results of Sec. III B for the case of an unperturbed free-draining coil [i.e., $\tau_{\text{trap}\pm}\to\tau_{0\pm}$ as given by Eq. (28)]. Note that Eq. (35) is valid strictly when $\varepsilon\ll\epsilon_\mu$ and thus Eq. (36) must be taken in the context of a linear approximation to the actual critical field.

IV. SIMULATION RESULTS

The simulation algorithm was written in C language. Simulations were carried out on both Sun and IBM UNIX computer workstations. The simulation parameters were $\rho=1$ for the radius of the semicircular protrusions and the periodicity of these protrusions was fixed at $|\Delta y|=3$. The springs were characterized by $N=5$ Kuhn segments, which leads to an unperturbed mean spring extension [14] of $\langle(\Delta r)^2\rangle_0\approx0.16$; from Eq. (18), it then follows that $r_{g0}\approx(M/37.5)^{1/2}$ and thus the unperturbed radius of gyration satisfies the conditions $2r_{g0}<|\Delta y|$ as well as $r_{g0}<\rho$ for $M<40$. Also, we set $\Delta\tau_{\max}=0.5$ and $m=1000$ for the maximum time increment and the damping parameter, respectively, in order to ensure against stochastic cooling. Finally, the walls have potentials characterized by $A=1$ and $\sigma=\rho/10=0.1$ [see Eq. (15)]; the maximum jump size allowed for any bead was thus conveniently set to $\sigma/4=0.025$ in order to lower the frequency of boundary condition violations (e.g., spring overextensions and jumping inside a wall protrusion).

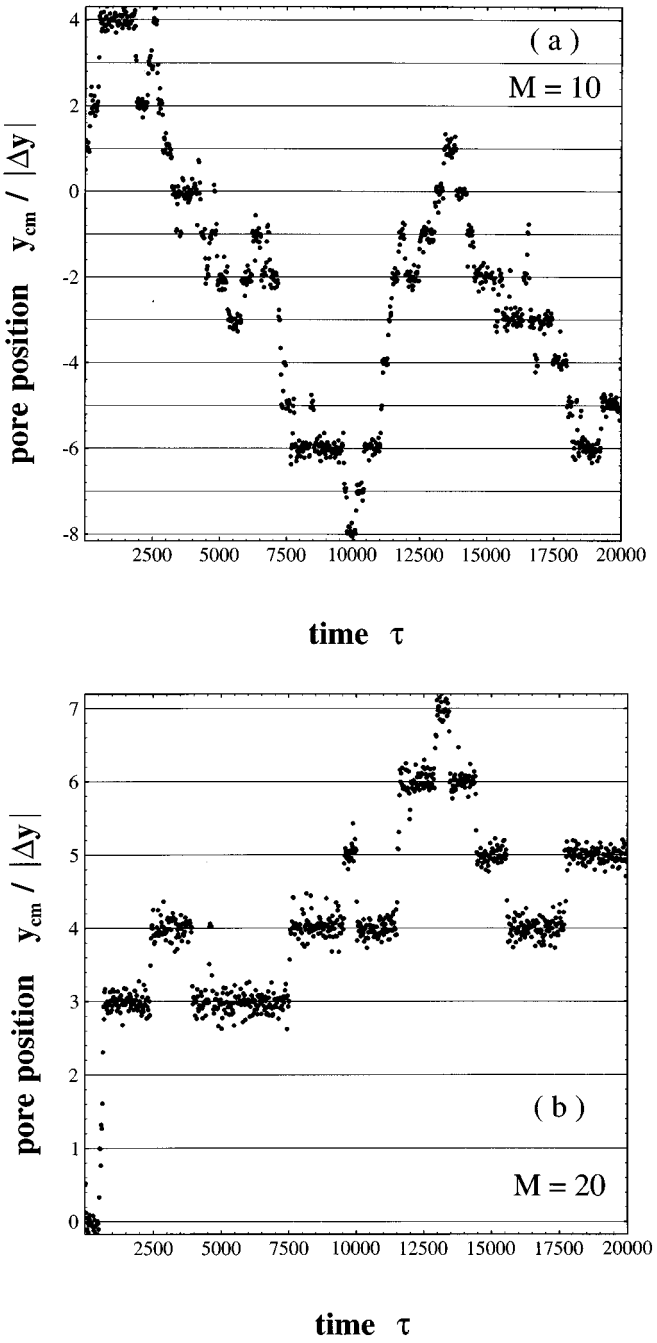

FIG. 4. Longitudinal position of the center of mass (scaled according to pore index $y_{\text{c.m.}}/|\Delta y|$) for two chains of differing molecular size M in the absence of an external field ($\varepsilon=0$) plotted as a function of time. In (a) we have a $M=10$ bead chain and in (b) we have a $M=20$ bead chain. Both migrate in tubes with characteristic diameters $d_T=2.8$ and $d_0=0.8$ with pores separated by a distance of $|\Delta y|=3$. The hoppinglike motion (i.e., from pore to pore) is indicative of an activated process that, in the case of $\varepsilon=0$, is purely entropically driven.

A. The zero-field case

In the case of zero electric field, the dynamics is regulated, in those cases where $r_{g0}>d_0$, by the entropic barriers and, consequently, the motion of the center of mass can be described as an unbiased hopping process as depicted in Fig. 4(a) for a $M=10$ bead chain within a tube of diameter

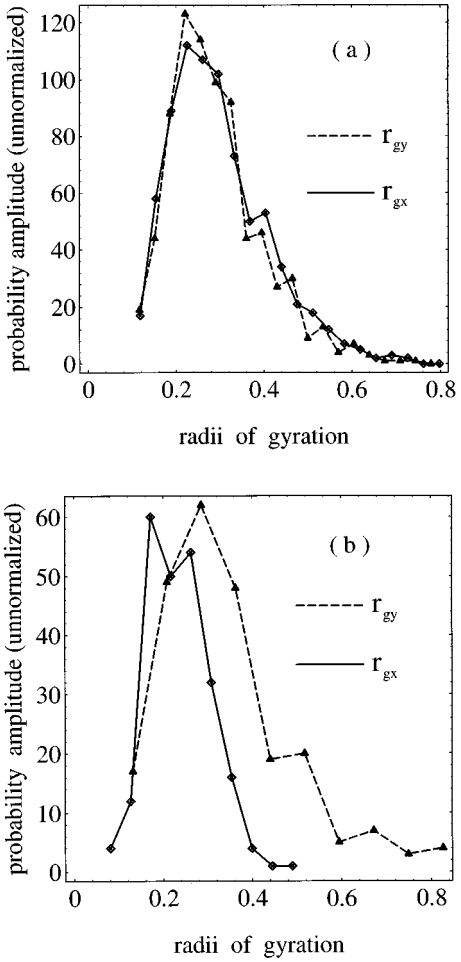

FIG. 5. Plotted are the distribution functions (in arbitrary units) for both the transverse and axial radii of gyration, r_{gx} and r_{gy}, for two ranges of the fractional pore position ($\mathscr{P}$) of the y component of the center of mass $y_{\text{c.m.}}$ of a $M=10$ bead polymer in the absence of an electric field ($\varepsilon=0$); this corresponds to Fig. 3(a). We define the fractional pore position as $\mathscr{P}=\min[k,1-k]$ with $k=[y_{\text{c.m.}}\text{mod}|\Delta y|]/|\Delta y|)$. When $\mathscr{P}\in[\frac{1}{3},\frac{1}{2}]$, the chain occupies the porelike regions of the tube where it is unperturbed. However, when $\mathscr{P}\in[0,\frac{1}{3}]$, which corresponds to stricture regions, the chain is squeezed in the transverse (x) direction and is simultaneously stretched in the longitudinal (y) direction.

$d_T=2.8$ (and thus $d_0=0.8$). We note that the molecule spends a proportionately small amount of time in the stricture regions (i.e., the jumps are quite fast) whereas, in the porelike regions (i.e., in the spatial voids), the time spent is much longer, as one might expect when entropic barriers are high. For a larger molecule, say with $M=20$ [Fig. 4(b)], the trapping within pores (voids) is more severe and the polymer thus spends proportionately more time trapped between the two stricture extremities of a pore. In Fig. 5 we plotted the distribution functions (in arbitrary units) for both the transverse and axial radii of gyration r_{gx} and r_{gy} for two ranges of the fractional pore position ($\mathscr{P}$) of the y component $y_{\text{c.m.}}$ of the position of the center of mass of a $M=10$ bead polymer; here we define the fractional pore position as $\mathscr{S}=\min[k,1-k]$ with $k=[y_{\text{c.m.}}\text{mod}|\Delta y|]/|\Delta y|$ and $|\Delta y|=3$. When $\mathscr{P}\in[\frac{1}{3},\frac{1}{2}]$, that is, when the chain is in the wide regions of the tube [Fig. 5(a)], both directions are spatially

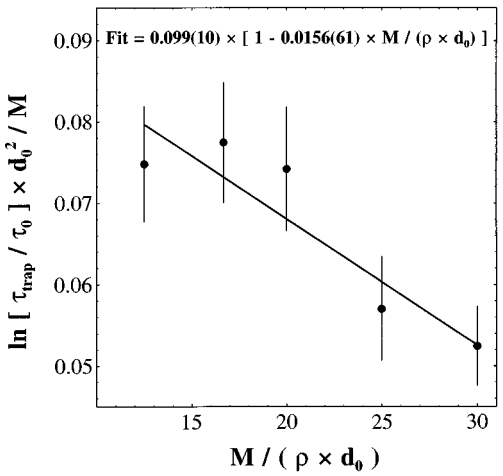

FIG. 6. Unconditional trapping time τ_{trap} plotted as a function of the (minimum) channel width d_0 for a field intensity $\varepsilon=0$. The vertical scale is $\ln[\tau_{\text{trap}}/\tau_0]d_0^2/M$ (τ_0 is the effective mean first passage time in the absence of strictures) while the horizontal scale is $M/\rho d_0$.

equivalent and we find $\langle r_{gx}\rangle\approx 0.30$ and $\langle r_{gy}\rangle\approx 0.29$ (with standard deviations $\Delta r_{gx}\approx\Delta r_{gy}\approx 0.11$). However, when $\mathscr{P}\in[0,1/3]$, which corresponds to being in a narrow channel [Fig. 5(b)], the chain is squeezed in the x direction (i.e., transverse to the tube axis) and we obtain $\langle r_{gx}\rangle\approx 0.24$ and $\langle r_{gy}\rangle\approx 0.34$ (with standard deviations $\Delta r_{gx}\approx 0.07$ and $\Delta r_{gy}\approx 0.15$). Thus the strictures cause the polymer chain to stretch in the tube (i.e., y) direction while simultaneously squeezing its perpendicular (x) component.

We now examine the scaling form of the unconditional trapping time τ_{trap} (defined as the mean first passage time between consecutive pore centers). According to Eq. (33), the scaled logarithmic ratio $\ln[\tau_{\text{trap}}/\tau_0]d_0^2/M$ [where τ_0 is the effective mean first passage time, given by Eq. (27), in the absence of strictures] versus $M/\rho d_0$ should reveal, to first order, a straight line with a slope $-\phi\theta$ and an intercept ϕ. However, since Eq. (33) is valid strictly for small $d_0/2\rho$ and $\theta M/\rho d_0$ ratios, we opted to fit only those data (see Fig. 6) that satisfied the conditions $d_0/2\rho<0.5$ and $\theta M/\rho d_0\leqslant 0.6$. The fit is reasonable and the resulting values for the topological parameters are found to be $\phi=0.099(10)$ and $\theta=0.0156(61)$.

B. Electrophoresis

Upon the application of an external electric field [see Figs. 7(a) and 7(b)], the hopping process becomes biased (forward jumps are favored) and the (forward) mean jumping time is reduced. This is especially true for field intensities above the critical field [i.e., $\varepsilon>\varepsilon_\mu(M)$, as shown in Fig. 7(b)] whose value we will now determine for various molecular sizes M.

The forward trapping time $\tau_{\text{trap}+}$ with respect to the field intensity ε is plotted in Figs. 8(a)–8(d), viz., $\ln[\tau_{\text{trap}+}/(2\tau_0)]/(M|\Delta y|)$ vs ε for molecules of size (a) $M=10$, (b) $M=20$, (c) $M=30$, and (d) $M=40$ for a channel with maximum diameter $d_T=2.8$ and minimum diameter $d_0=0.8$. Superposed on these graphs is the predicted

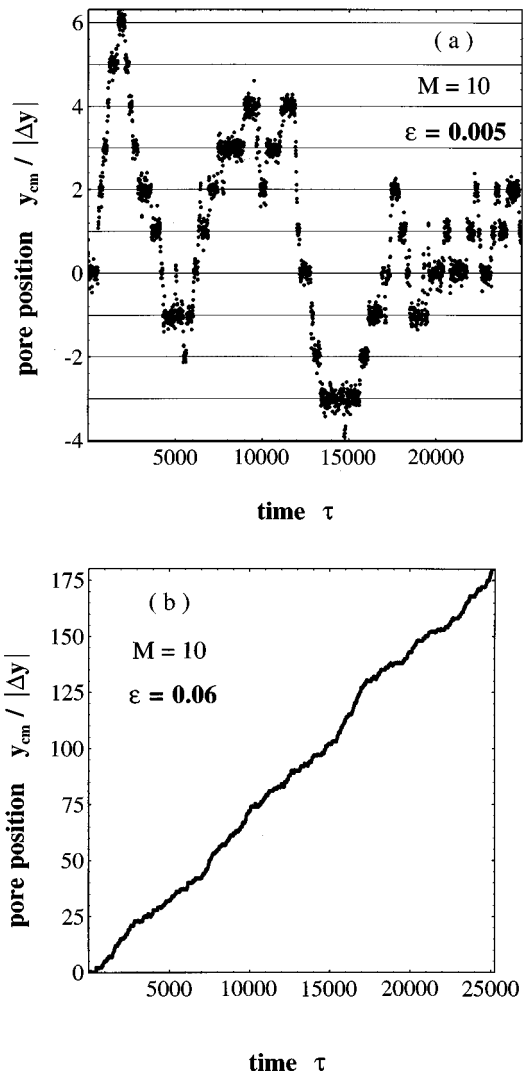

FIG. 7. Longitudinal position of the center of mass (scaled according to pore index $y_{\text{c.m.}}/|\Delta y|$) for a $M=10$ bead chain in a tube with characteristic diameters $d_T=2.8$ and $d_0=0.8$ plotted (pore index vs time) for a field intensity (a) $\varepsilon=0.005<\varepsilon_\mu$ and (b) $\varepsilon=0.06>\varepsilon_\mu$, where $\varepsilon_\mu(M=20)=0.039(6)$.

(dashed) line $\varepsilon-\varepsilon_\mu(M)$ valid for $\varepsilon\ll\varepsilon_\mu(M)$. This expression was found from substitution of the fitted topological parameters θ and ϕ (from Fig. 6) into Eq. (36); the critical field is thus predicted to obey $\varepsilon_\mu(M)\approx 0.052(5)\times[1-M/64(25)]$. The predicted line (dashed) is indeed in reasonable agreement with the simulation data for field intensities $\varepsilon\ll\varepsilon_\mu(M)$, but underestimates the trapping time for larger field intensities; this is largely due to the saturation limit of $\tau_{\text{trap}+}$ as given by Eq. (28). Note the poor agreement between the predicted behavior and the data for the $M=40$ bead chain. This was anticipated since the free radius of gyration r_{g0} is now larger than the radius of the semicircular protrusions ρ and thus the $M=40$ bead chain does not quite meet the criteria (i.e., $r_{g0}(M)<\rho$) for which Eq. (31) is valid. The critical field intensities, manifested as the field intensity for which the best fit (solid) curve crosses the field axis, can be fitted linearly (to a good approximation) with respect to M (see Fig. 9) as predicted from Eq. (36); the best straight line fit through our critical field intensities yields the relation $\varepsilon_\mu(M)\approx 0.057(3)[1-M/71(15)]$ (see Fig. 9). Our simple analytical model thus provides an adequate description of the physics of electrophoresis in entropically inhomogeneous media.

C. Phase diagram for entropic trapping

We now present a phase diagramlike description of the entropic trapping of a polyelectrolyte. In Fig. 10 we give our simulation results for a $M=10$ bead chain migrating in a tube with diameters $d_T=2.8$ and $d_0=0.8$. We plotted the logarithm of the relative forward trapping time $\log_{10}[\tau_{\text{trap}+}/(2\tau_0)]$ versus the logarithm of relative reciprocal field strength $\log_{10}[\varepsilon_\mu/\varepsilon]$. The solid line is the prediction for the limiting case of a free chain $\log_{10}[\tau_{0+}/(2\tau_0)]$, where τ_{0+} is given by Eqs. (26)–(28). Three separate regimes can be identified: (a) a high field asymptotic regime where the forward trapping time approaches the free-chain limit (note the unit slope), (b) a transition regime around the critical field, and, finally, (c) a plateau regime for vanishing field intensities $\varepsilon\ll\varepsilon_\mu$, where the dynamics is dominated by entropic effects. The distance between the plateau and the limiting curve (the horizontal part of the solid line) can be taken as a quantitative measure of the degree of entropic trapping. This distance for fields larger than the critical field can be regarded as a measure of the friction (induced through collisions with the strictures) against the motion of the chain. The critical field is shown to be that field for which the (forward) trapping time decrease below the transit time $2\tau_0$ predicted for a free chain in the vanishing-field limit; thus the critical field appears at the intersection point (0,0). Understanding how this diagram varies for different molecular sizes and stricture geometries is obviously the key to optimizing a polymer separation system that uses inhomogeneous sieving media [21]. This is planned to be discussed in a forthcoming article.

D. Longitudinal diffusion coefficient $d_{\text{cm}\|}$ for $\varepsilon>\varepsilon_\mu$

Above the critical field ε_μ, the hopping mechanism can be modeled as a directed walk (here in one dimension) with a mean jumping time $\langle\tau_{\text{trap}+}\rangle$ and a fixed jump size $|\Delta y|$. In this limit, the variance of the (forward) jumping time $\sigma^2_{\text{trap}+}=\langle\tau^2_{\text{trap}+}\rangle-\langle\tau_{\text{trap}+}\rangle^2$ may be related to the longitudinal diffusion coefficient $d_{\text{c.m.}\|}$ via the expression [22]

$$d_{\text{c.m.}\|}\approx\frac{|\Delta y|^2}{2}\frac{\sigma^2_{\text{trap}+}}{\langle\tau_{\text{trap}+}\rangle^3}. \tag{37}$$

In Fig. 11 we have plotted the longitudinal diffusion coefficient $d_{\text{c.m.}\|}$, as given by Eq. (37), vs $\log_{10}(\varepsilon)$ for a $M=10$ bead chain in a tube with characteristic diameters $d_T=2.8$ and $d_0=0.8$. We find that there exists a critical field intensity $\varepsilon_D(M=10)\approx 0.2$ at which the diffusion coefficient $d_{\text{c.m.}\|}$ reaches a maximum value. Our results (not shown) indicate that $\varepsilon_D(M)$ is a decreasing function of molecular size M, as expected. This implies the existence of an intermediate regime between the low field ($\varepsilon<\varepsilon_\mu$) regime, dominated by entropic trapping, and the high-field ($\varepsilon>\varepsilon_D$) regime, which is characterized by the (almost) free electrophoretic drift of the chain. In the intermediate field regime ($\varepsilon_\mu<\varepsilon<\varepsilon_D$), the transitions are all in the direction of the field since the elec-

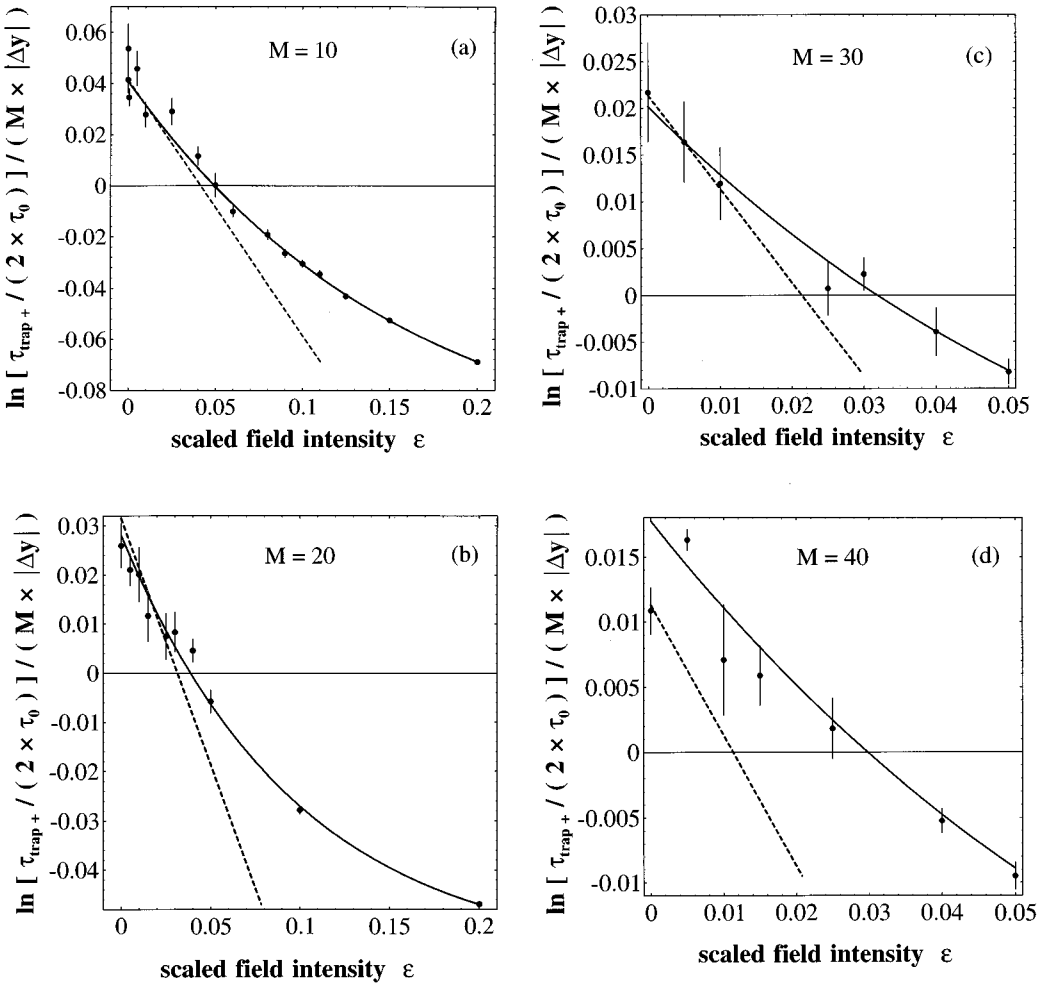

FIG. 8. Forward trapping time $\tau_{\text{trap}+}$ plotted as $\ln[\tau_{\text{trap}+}/(2\tau_0)]/(M|\Delta y|)$ versus ε for molecular sizes (a) $M=10$, (b) $M=20$, (c) $M=30$, and (d) $M=40$. Superposed is the predicted behavior $\varepsilon_\mu(M)-\varepsilon$ for small field intensities $\varepsilon \ll \varepsilon_\mu(M)$ where one has $\varepsilon_\mu(M)=0.057(3)[1-M/71(15)]$ as found from the zero-field data of Fig. 5. Note that the agreement is excellent for $M<40$, while for $M=40$ the agreement is poor due to the fact that the radius of gyration then becomes larger than the radius of the semicircular protrusions.

tric field induces Coulomb forces that are much stronger than the entropic forces on the chains; however, as the detrapping process is still sufficiently random (i.e., the distribution of detrapping times $\tau_{\text{trap}+}$ is still relatively broad), a large spatial dispersion of the molecules results over time.

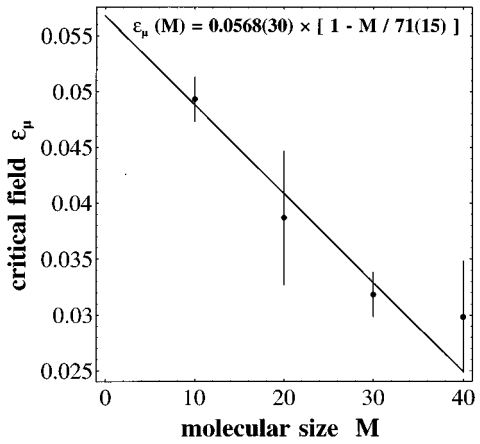

FIG. 9. Critical field ε_μ plotted vs molecular size M for the cases shown in Fig. 8.

In Fig. 12 we propose a schematic of the phase diagram for electrophoretic entropic trapping; depicted is the molecular size M as a function of scaled field intensity ε. We see three different regions bounded by the two critical lines $\varepsilon_\mu(M)$ and $\varepsilon_D(M)$. In region I ($\varepsilon<\varepsilon_\mu$), we are in the entropic trapping regime and the field plays a minor "biasing" role. In region III ($\varepsilon>\varepsilon_D$), we enter the free electrophoretic drift (high field) regime where the entropic potentials play a minor "frictional" role. Region II ($\varepsilon_\mu<\varepsilon<\varepsilon_D$) is the intermediate crossover regime where the field can overcome the effect of entropic trapping on the mobility μ, but not its effect on the longitudinal diffusion coefficient $d_{\text{c.m.}||}$. Because the two critical lines $M(\varepsilon_\mu)$ and $M(\varepsilon_D)$ have finite negative slopes on the diagram, the optimum field intensity for a polydisperse sample, bounded by molecular sizes $M_1<M<M_2$, is given by $\varepsilon \approx \varepsilon_\mu(M_2)$ with $\varepsilon \ll \varepsilon_D(M_2)$ since we do not want the electrophoretic bands to smear out [e.g., choosing $\varepsilon \approx \varepsilon_\mu(M_1)$ would prove disastrous and no separation would be possible]. This represents a limiting criterion for separation to be possible in such systems. Note that in the high field regime $\varepsilon>\varepsilon_D(M_1)$, the mobility μ is of the order of unity for all species and separation is minimal. Thus the existence of the intermediate regime, where the longitu-

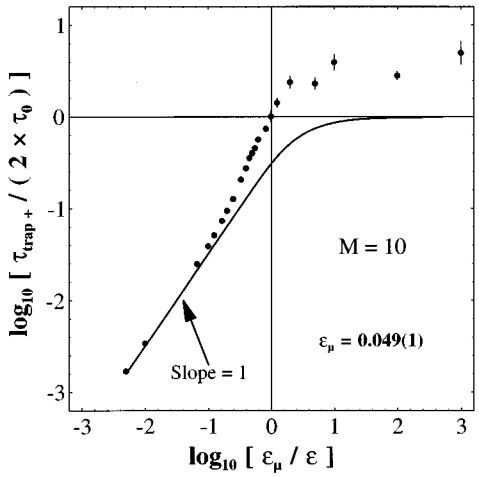

FIG. 10. Phase diagram for a $M=10$ bead chain in a tube of diameter $d_T=2.8$ and of channel diameter $d_0=0.8$. Here we plot the logarithm of the (relative) forward trapping time $\log_{10}[\tau_{\text{trap}+}/(2\tau_0)]$ versus the logarithm of (relative) reciprocal field strength $\log_{10}[\varepsilon_\mu/\varepsilon]$. The solid line represents the limiting (free-drift) behavior of polyelectrolytes in the absence of constraints $\log_{10}[\tau_{0+}/(2\tau)]$, where τ_{0+} is given by Eqs. (26)-(28).

dinal diffusion coefficient becomes catastrophically large, limits the prospects of being able to use entropic trapping as a means of obtaining high resolution electrophoretic separation of polyelectrolytes.

V. CONCLUSION

It was demonstrated by Baumgärtner and Muthukumar [8–10] that a series of open spaces (pores) and confinements

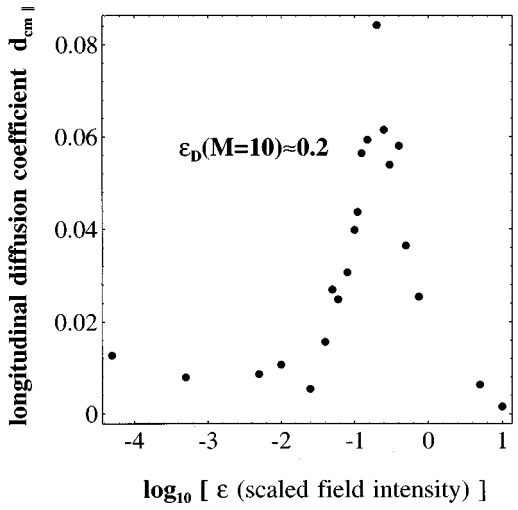

FIG. 11. Longitudinal diffusion coefficient $d_{\text{c.m.}||}$ plotted as a function of the base 10 logarithm of the field intensity ε for a $M=10$ bead chain in a tube with diameters $d_T=2.8$ and $d_0=0.8$. Note the existence of a critical field intensity $\varepsilon_D\approx 0.2$ for which $d_{\text{c.m.}||}$ is a maximum. The rise from a zero-field value of $d_{\text{c.m.}||}\approx 0.01$ to $d_{\text{c.m.}||}\approx 0.084$ represents more than an eightfold increase.

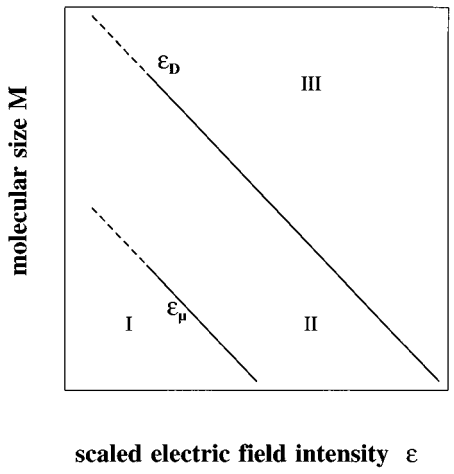

FIG. 12. This schematic phase diagram of molecular size M vs field intensity ε reveals three regions bounded by the two lines showing the molecular size-dependent critical fields $\varepsilon_\mu(M)$ and $\varepsilon_D(M)$. In region I, we are in the entropic trapping regime. Region II is an intermediate regime where the applied electric field dominates over the entropic effects. Finally, in region III, we enter the free electrophoretic drift regime where the strictures merely provide ''frictional resistance.''

(strictures), for which the stricture size is of the order of the dimensions of the polymeric coil, are thermodynamically equivalent to entropic traps and entropic barriers, respectively. The strictures create entropic barriers possessing a height that controls the rate of transport between the pores. In this paper, we considered the effect of electric fields on the entropic trapping process in a model system; we revealed the existence of three electrophoretic regimes for molecular species that can be fully contained within the pores and stricture regions. The special case where the polyelectrolytes are distributed over many pores was not considered. Such a study would prove most interesting, especially if one can observe a transition to the reptation regime (e.g., species whose radii of gyration are in excess of, say, 2–5 times the average pore spacing are reputed to undergo such transitions [23]).

We have shown that, in our model system of pores and ''round'' strictures, the electrophoretic transport of polyelectrolytes is an activated process whereby the rate of entropic barrier passage is controlled by the product of the attempt frequency with an exponential in both (i) the chain's entropy decrease during confinement inthe barrier and (ii) the drop in electric potential energy. This has important consequences in our understanding of Ogston sieving dynamics of DNA gel electrophoresis as one expects a transition from the Ogston sieving regime to that of entropic barriers.

We also demonstrated the existence of a critical (mobility) field intensity, ε_μ, which we related to the characteristics of two different phase diagrams. These diagrams not only obviate the different transport regimes, they also serve to characterize the degree of entropic trapping in both a qualitative as well as a quantitative fashion for the given experimental setup. Note that the existence of a critical (mobility) field ε_μ for single-stranded DNA (ssDNA) was verified experimentally through the studies of Mayer, Slater, and Drouin [13] in polyacrylamide gels; it was found that, for ssDNA

below 1000 bases, a field intensity of 19 V/cm is beyond the critical field ε_μ and, for molecular sizes of the order of $M=400$ bases, the critical field is $\varepsilon_\mu(400 \text{ bases}) \approx 9.4$ V/cm. An extensive experimental investigation of $\varepsilon_\mu(M)$ is in progress [24].

We note that, in our nonexcluded volume model, the critical field $\varepsilon_\mu(M)$ is molecular size dependent due to the topological interaction between the polymer chain and the (round) stricture; were the stricture flat and long enough to fully contain the chains (no spillout), this molecular size dependence would disappear (self-excluded-volume interactions would not alter this conclusion). However, in the strong confinement limit where spillout of the monomers occurs, the work of Baumgärtner and Muthukumar [9] would suggest the scaling relationship

$$\frac{\tau_{\text{trap}\pm}}{2\tau_0} \approx \exp\left\{ M\left[f\left(\frac{1}{d_0}\right)^{1/\nu} - \frac{1}{2}(f+1)\left(\frac{1}{d_T}\right)^{1/\nu} \mp \boldsymbol{\varepsilon}|\Delta y| \right]\right\}, \tag{38}$$

where f is the fraction of monomers inside the stricture during the transition and ν is Flory's exponent ($\nu=\frac{3}{4}$ and $\nu\approx\frac{3}{5}$ in $d=2$ and 3 dimensions, respectively). By strong confinement, we mean that the pores are large enough to fully contain the chains between transitions while, during transitions, only a fraction f of the beads are confined within the stricture and the remaining $(1-f)M$ beads are distributed over the two adjacent pores. Equation (38) applies strictly for a self-excluded-volume chain in a ''toy model'' network comprised of pores of size d_T and of strictures of diameter d_0 and length λ. In this limit, f is molecular size dependent and given by

$$f \approx \lambda d_0^{(1/\nu)-1} M^{-1}. \tag{39}$$

Consequently, we may rewrite Eq. (38) in the form

$$\frac{\tau_{\text{trap}\pm}}{2\tau_0} \approx \exp\{M|\Delta y|[(\boldsymbol{\varepsilon}_\mu(M) \mp \boldsymbol{\varepsilon}]\}, \tag{40}$$

where the molecular size-dependent critical (mobility) field is now given by

$$\boldsymbol{\varepsilon}_\mu(M) \approx \frac{1}{M|\Delta y|}\left[n_b - \frac{1}{2}\left(n_b + \frac{M}{d_0^{1/\nu}}\right)\left(\frac{d_0}{d_T}\right)^{1/\nu}\right], \tag{41}$$

where the topological parameter $n_b=\lambda/d_0$ may be regarded as the number of ''blobs'' contained in the stricture during a transition (as per the scaling argument). We thus conclude that a molecular size-dependent critical field $\varepsilon_\mu(M)$ is a general feature of any realistic entropic trapping system.

Interestingly, as entropic trapping is an activated process, it may be possible to exploit stochastic-resonance effects [25] in entropic trapping systems; one would then require that the pulse duration (of the ac component of the field) be set to conform with the time between traps (i.e., $\tau_{\text{pulse}} \approx \tau_{\text{trap}}$). It is not unreasonable, then, to suspect that such resonance effects play a major role in techniques such as field-inversion gel electrophoresis, where great improvements in the resolution of electrophoresed molecular bands is possible over other techniques [26,27].

It is indeed the competition between the mobility and the diffusion coefficient (over the range of applicable field intensities) that will determine the resolution in entropic trapping systems. In our model system and for field intensities below the critical field ε_μ, the mobility is very molecular size dependent, but, in fact, small; when the field intensity exceeds the critical field ε_D, the mobilities approach unity; for intermediate field intensities $\varepsilon_\mu < \varepsilon < \varepsilon_D$, band broadening becomes a limiting factor due to the large diffusion coefficient. The existence of the, as of yet, unknown intermediate regime II (see Fig. 12) renders entropic trapping an unlikely mechanism for high-performance separation systems if pulsed fields are not used.

Relaxation phenomena, although not discussed explicitly in this article, also play a role in entropic trapping systems during electrophoresis experiments. For instance, one typically requires fairly large fields to minimize the duration of the separation. Unfortunately, the maximum field strength permitted by an entropic separation process is in fact limited due to the finite relaxation times of polymeric coils, which, upon emerging from a stricture, remain somewhat perturbed (collapsed) over finite (relaxation) time scales. Indeed, for large field intensities, the free-drift time between strictures can in fact be less than the relaxation time. This engenders, therefore, yet another critical (relaxation) field intensity [17], which, for Rouse-like relaxation, scales as $\varepsilon_{\text{relax}} \sim |\Delta y|/M^2$, where $|\Delta y|$ is the interpore distance. Of course, one must ensure that the field intensity is kept below this relaxation critical field in order to remain in the entropic trapping regime (the conformational entropy is indeed linked with the relaxation of the chain). A further development along these lines is planned to appear in a forthcoming study.

ACKNOWLEDGMENTS

The authors would like to thank P. Mayer, G. Drouin, Jean Rousseau, J. -L. Viovy, D. Hoagland, M. Muthukumar, and B. Zimm for many fruitful discussions concerning entropic trapping. This work was supported by a Research Grant from NSERC to G.W.S.

[1] T. D. Yager, T. E. Zewert, and L. E. Hood, Acc. Chem. Res. **27**, 94 (1994).

[2] E. Arvanitidou, D. Hoagland, and D. Smisek, Biopolymers **31**, 435 (1991).

[3] M. Doi and S. K. Edwards, *The Theory of Polymer Dynamics*, International Series of Monographs on Physics · 73 (Oxford University Press, Oxford, 1986).

[4] O. J. Lumpkin, P. Déjardin, and B. H. Zimm, Biopolymers **24**, 1573 (1985).

[5] G. W. Slater and J. Noolandi, Phys. Rev. Lett. **55**, 1579 (1985).

[6] J. M. Deutsch, J. Chem. Phys. **90**, 7436 (1989).
[7] S. P. Obukhov and M. Rubinstein, J. Phys. (France) II **3**, 1455 (1993).
[8] A. Baumgärtner and M. Muthukumar, J. Chem. Phys. **87**, 3082 (1987).
[9] A. Baumgärtner and M. Muthukumar, Macromolecules **22**, 1937 (1989).
[10] M. Muthukumar and A. Baumgärtner, Macromolecules **22**, 1941 (1989).
[11] M. Muthukumar, J. Non. Cryst. Solids **131-133**, 654 (1991).
[12] D. Hoagland and M. Muthukumar, Macromolecules **25**, 6696 (1992).
[13] P. Mayer, G. W. Slater, and G. Drouin, Appl. Theor. Electroph. **3**, 147 (1993).
[14] G. W. Slater, S. J. Hubert, and G. I. Nixon, Macromol. Theory Simul. **3**, 695 (1994).
[15] E. O. Shaffer II and M. Olvera de la Cruz, Macromolecules **22**, 1351 (1989).
[16] G. I. Nixon and G. W. Slater, Phys. Rev. E **50**, 5033 (1994).
[17] G. I. Nixon, M. Sc. thesis, University of Ottawa, 1994 (unpublished).
[18] P. J. Flory, *Statistical Mechanics of Chain Molecules* (Interscience, New York, 1969).
[19] G. W. Slater, J. Rousseau, and J. Noolandi, Biopolymers **26**, 863 (1987).
[20] P. G. de Gennes, *Scaling Concepts in Polymer Physics* (Cornell University Press, Ithaca, 1979).
[21] J. Rousseau, P. Mayer, G. W. Slater, and G. Drouin (unpublished).
[22] J. P. Bouchaud and A. Georges, C. R. Acad. Sci. Paris, Ser. 2, **307**, 1431 (1988).
[23] E. Arvanitidou, D. Hoagland, and D. Smisek, Biopolymers **31**, 435 (1991).
[24] G. Drouin, J. Rousseau, G. W. Slater, and P. Mayer (unpublished).
[25] B. McNamara and K. Wiesenfeld, Phys. Rev. A **39**, 4854 (1989).
[26] G. F. Carle, M. Frank, and M. V. Olson, Science **232**, 65 (1986).
[27] C. Turmel, É. Brassard, G. W. Slater, and J. Noolandi, Nucl. Acids Res. **18**, 569 (1990).